On the effects of aggregate sieving in the shielding and thermo-mechanical performance of concrete

J. Zhang[1], B. Pomaro[1], G. Mazzucco[1], B.F. Dongmo[1], C.E. Majorana[1] and V.A. Salomoni[1,2]

[1]Department of Civil, Environmental and Architectural Engineering, University of Padova, Italy.
[2]Department of Management and Engineering, University of Padova, Vicenza, Italy.

Abstract

In this paper, the influence of aggregate sieving and distribution on the shielding performance of concrete against nuclear radiation is investigated numerically. A thermo-mechanical and neutron diffusion coupled numerical formulation is proposed to address the specific problem related to irradiated concrete. This model solves the multi-physics problem by combining a two-group neutron diffusion theory, with the thermal conduction equation adapted to the radiation condition, and the mechanical equilibrium problem. Concrete is modeled at the mesoscale as a two-phase material, comprising mortar matrix and aggregates. Three grading curves of Fuller type are simulated, different for the nominal diameter size intervals of the polyhedral aggregates, which are randomly distributed within cubic samples of concrete composite material. A boron-rich material, colemanite, is utilized as aggregate in the numerical simulations. The results show that the fast neutron flux is not much influenced by the variation of the grading curves. On the other hand, a slight variation of the coarse aggregate volume fraction is found to affect to some extent the thermal flux. As regards temperature and stress distribution, it is noted the barrier effects that the inclusions bring to the state variable diffusion process.

Keywords: Thermo-mechanical, neutron diffusion, coupled problems, Finite Elements, mesoscale modeling, irradiated concrete.

1 Introduction

Concrete is widely used as a shielding material against radiation. This is attributed to its excellent shielding, mechanical properties, fairly heat resistance, and low cost [1]. Moreover, its mix design can be improved to contain in optimal amount light elements (hydrogen, through its water content) to attenuate neutrons, and heavy ones (e.g. barytes, ilmenite, and iron-bearing aggregates, etc.) to absorb secondary gamma rays [2, 3]. In this regard, comparative studies have been conducted regarding the shielding performance of concrete with different aggregate materials [4, 5].

Among all ionizing radiations, the shielding of neutrons is the most challenging task, due to their electrical neutrality, which permits them to penetrate deeper into matter. Studies have reported that neutron radiation has detrimental effects on concrete mechanical properties when the fast neutron fluence (E $>$ 0.1 MeV) reaches $1.0 \times \ 10^{19}$ n/cm^2 [1]. In this scenario the primary mechanism is confirmed to be radiation induced volume expansion (RIVE) at the level of aggregates [5]. Within the shielding walls of nuclear facilities the neutron flux is not uniformly distributed. The evaluation of damage triggering and propagation in irradiated concrete members demands a precise prediction of the neutron flux distribution on concrete structures [6]. Further, in the shielding process radiation energy is partially transformed into heat, which leads to temperature rise and additional damage [7]. Therefore, the prediction of radiation induced heat rise, and temperature distribution is compulsory to tackle the multiphysics of the problem.

The role of aggregates in affecting concrete mechanical properties and durability has been object of deep study [8, 9]. Aggregate sieving is also investigated in relation to drying shrinkage, and fracture behaviors [10, 11]. Regarding the influence of the aggregate grading curve on concrete shielding performance, it is reported that an optimum sieving can increase the material shielding properties, as a result of a reduced porosity [12].

In this work, the influence of aggregate distribution and grading curve on the shielding and thermo-mechanical behaviour of concrete is investigated numerically by means of a coupled thermo-mechanical and neutron diffusion (TMN) formulation. Analyses are conducted at the mesoscale, where aggregates are distributed randomly in the sample, following Fuller curves with different diameter size intervals. In Section 2.1 the mathematical and numerical model are elucidated; in Section 2.2 the approach used to generate the solid models at the scale of concrete constituents is illustrated. Section 3 completes the work with pertinent numerical results.

2 Materials and methods

2.1 Thermo-mechanical and neutron diffusion coupled model

A deterministic approach is adopted in this work to simulate the neutron transport process. Due to the fact that fast neutrons and thermal neutrons have different effects on concrete (RIVE and temperature rise, respectively), a cut-off value of 0.1 MeV is set to divide neutrons with different kinetic energies. Along this line, the real neutron spectrum is simplified into a two-group system. Each one of the two groups is attributed a specific neutron diffusion equation

$$\frac{1}{v_1}\frac{\partial \phi_1}{\partial t} - \nabla^{\mathrm{T}}\left(\boldsymbol{D}_1 \nabla \phi_1\right) + \Sigma_{R_1}\phi_1 = 0 \tag{1}$$

$$\frac{1}{v_2}\frac{\partial \phi_2}{\partial t} - \nabla^{\mathrm{T}}\left(\boldsymbol{D}_2 \nabla \phi_2\right) + \Sigma_{a_2}\phi_2 = \Sigma_{S_{12}}\phi_1, \tag{2}$$

where subscripts $i = 1, 2$ are used to differentiate the fast and the thermal group, respectively; ϕ_i is the scalar neutron flux; v_i is the neutron speed; t is time; $\boldsymbol{D}_i$ is the neutron diffusion coefficient tensor; Σ_{R_1} is the effective removal cross section of the fast group; Σ_{a_2} is the macroscopic absorption cross section of the thermal group; $\Sigma_{S_{12}}$ is the fast-to-thermal-group-transfer cross section.

To cope with uneven temperature distribution in concrete structures caused by radiation, the classic heat conduction equation is adopted

$$\rho c_p \frac{\partial T}{\partial t} = \nabla^{\mathrm{T}}(\mathbf{k}\nabla T) + Q, \tag{3}$$

where T is temperature, c_p the specific heat capacity, ρ the mass density, $\mathbf{k}$ the thermal conductivity tensor, and Q the volumetric heat source. It is noted that the term Q accounts for the heat released by the thermal neutrons during the capture process involving them, while being absorbed in the shielding medium. It is defined as

$$Q = 1.6 \times 10^{-13} \Sigma_c \mathcal{E}_b \phi_2, \tag{4}$$

where Σ_c is the macroscopic neutron capture cross section, and $\mathcal{E}_b$ the binding energy for the capture process. This term specifically accounts for the coupling between the thermal neutron diffusion and the thermal problem.

If inertial forces are neglected, the equation of mechanical equilibrium in small-strain theory yields

$$\mathbf{L}^{\mathrm{T}}\boldsymbol{\sigma} + \rho\mathbf{g} = \mathbf{0}, \tag{5}$$

where $\boldsymbol{\sigma}$ is the Cauchy stress vector; $\mathbf{g}$ is the gravity acceleration, so that $\rho\mathbf{g}$ is the body force per unit volume; $\mathbf{L}$ is the well-known differential operator. In linear elasticity: $\boldsymbol{\sigma} = \mathcal{D}\boldsymbol{\varepsilon}^{\mathrm{e}}$, with $\mathcal{D}$ the constitutive elastic tensor.

The total strain $\boldsymbol{\varepsilon}$ is regarded as the sum of the elastic strain component $\boldsymbol{\varepsilon}^{\mathrm{e}}$, the thermal strain component $\boldsymbol{\varepsilon}^{\mathrm{th}}$, and the radiation induced component due to RIVE $\boldsymbol{\varepsilon}^{\mathrm{RIVE}}$; namely

$$\boldsymbol{\varepsilon} = \boldsymbol{\varepsilon}^{\mathrm{e}} + \boldsymbol{\varepsilon}^{\mathrm{th}} + \boldsymbol{\varepsilon}^{\mathrm{RIVE}}. \tag{6}$$

The thermal strain component is given by

$$\boldsymbol{\varepsilon}^{\mathrm{th}} = \mathbf{I}\alpha\left(T - T_0\right), \tag{7}$$

where T_0 is the initial temperature; α is the thermal expansion coefficient of the medium; and $\mathbf{I} = \begin{bmatrix} 1 & 1 & 1 & 0 & 0 & 0 \end{bmatrix}^{\mathrm{T}}$ is the identity vector, which accounts for an isotropic strain evolution. The estimated RIVE strain component is defined by [4]

$$\boldsymbol{\varepsilon}^{\mathrm{RIVE}} = \mathbf{I}\kappa\boldsymbol{\varepsilon}_{\max}\frac{e^{\delta\Phi} - 1}{\boldsymbol{\varepsilon}_{\max} + \kappa e^{\delta\Phi}}, \tag{8}$$

where $\boldsymbol{\varepsilon}_{\max}$, κ, and δ are material parameters calibrated over length change measurements of irradiated concrete specimen made of different aggregates. In Eq. (8) Φ is the neutron fluence, which can be obtained by integration on the irradiation times of the fast group neutron flux, i.e.: $\Phi = \int_0^t \phi_1 dt$.

2.2 Mesoscale modeling of concrete

The heterogeneity of concrete is considered via a mesoscale modeling approach, where coarse aggregate inclusions are explicitly modeled within the cement paste matrix. To regularly round or ellipsoidal shapes of aggregates, a polyhedral shape is preferred to model inclusions, in reason of the evidence, pointed out by previous studies of some of the authors [13, 14], of a conceivable stress localization in concrete, affected by the irregular aggregate shape. The reader is referred to [15] for an extensive illustration of the random distribution algorithm used to effectively distribute aggregates within the reference domain of the sample, in agreement with a specific grading curve, and excluding overlapping [15]. An example of the two-phase solid model generated with this procedure is shown in Figure 1.

It is assumed that the aggregate sieving follows the Fuller grading curve, which is acknowledged to achieve optimum packing, while ensuring a good workability

$$P(d) = 100\left(\frac{d}{d_{\max}}\right)^n. \tag{9}$$

In Eq. (9) $P(d)$ is the cumulative percentage passing a sieve with diameter d; $d_{\max}$ is the maximum diameter of the aggregates; n is the characteristic exponent of the equation ($n = 0.5$). To account for the minimum size of aggregates, $d_{\min}$, the cumulative aggregate percentage within the grading segment $[d_{\min}, d]$ is computed as

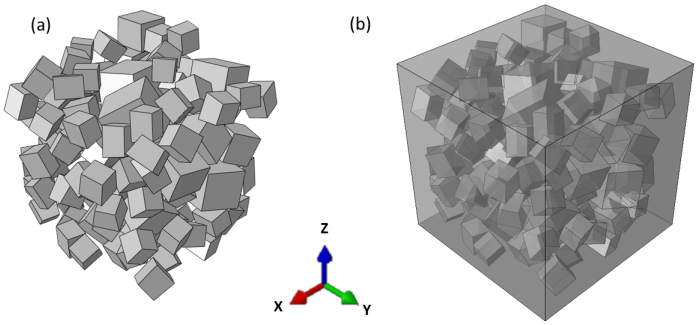

Figure 1: Mesoscale model of concrete: (a) aggregates; (b) matrix.

$$P\left(d_{\min}, d\right) = \frac{d^n - d_{\min}^n}{d_{\max}^n - d_{\min}^n}, \quad d \in \left[d_{\min}, d_{\max}\right]. \tag{10}$$

The dimension of the cubic sample is chosen as 50 mm. Three ranges of aggregate size are considered. They are respectively: [4.75, 12.5], [4.75, 9.5], and [2.36, 4.75] mm. Three models (labeled as Model-1 to -3) corresponding to the three aforementioned nominal diameter size intervals are generated. For each of them the simulated grading curve is compared to the theoretical Fuller curve obtained by Eq. (10) in Figure 2. It is remarked that all curves are consistent to the target one, as expected. It is noteworthy that the aggregate volume fraction of Model-1 and Model-2 are 30.5%; and that of Model-3 is 30%. This discrepancy with respect to the target value of 30% is attributed to the numerical approximation error between the input target volume fraction, and that obtained via the random distribution algorithm mentioned at Section 2.2. This discrepancy is relevant to the numerical results discussion that follows.

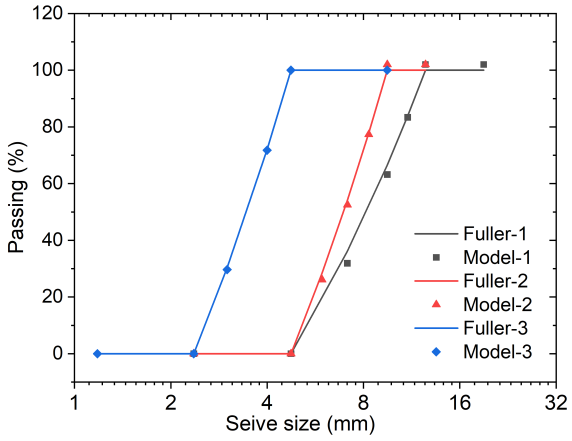

Figure 2: Considered grading curves for the numerical analyses. Comparison between simulated and target curves for three different intervals of nominal diameter size.

Colemanite aggregate are considered in the numerical analyses. This kind of ag-

gregate is particularly suitable for radiation shielding applications because of its high content in boron, which is a light material, effective in absorbing thermal neutrons without producing highly penetrating gamma rays as by-product. The shielding properties of colemanite aggregate and mortar matrix are calculated based on their corresponding chemical composition [16, 17], while their thermal and mechanical properties are taken from [18, 19]. The material parameters used in the numerical analyses are summarized in Table 1.

Variables	Units	Cement Paste	Aggregate
E	$[\mathrm{MPa}]$	32500	49700
v	$[-]$	0.2	0.2
α	$[^{\circ}\mathrm{C}^{-1}]$	9.0×10^{-06}	1.1×10^{-05}
k	$[\mathrm{W}/(\mathrm{cm}\cdot{}^{\circ}\mathrm{C})]$	0.019	0.085
ρ	$[\mathrm{kg/cm^3}]$	0.0024	0.0027
c_p	$[\mathrm{J}/(\mathrm{kg}\cdot{}^{\circ}\mathrm{C})]$	813	757
D_1^+	$[\mathrm{cm}]$	2.7312	2.2889
D_2^+	$[\mathrm{cm}]$	0.9718	0.0268
$\Sigma_{R_1}^+$	$[\mathrm{cm}^{-1}]$	0.0856	0.1039
$\Sigma_{S_{12}}^*$	$[\mathrm{cm}^{-1}]$	0.0856	0.1039
$\Sigma_{a_2}^+$	$[\mathrm{cm}^{-1}]$	0.0229	11.9838
Σ_c^*	$[\mathrm{cm}^{-1}]$	0.0229	11.9838
$\mathcal{E}_b^*$	$[\mathrm{MeV}]$	8.0	8.0

* Value is assumed;

+ Value is calculated.

Table 1: Thermo-mechanical and shielding parameters for the materials used in the numerical analyses.

3 Numerical results

For each solid model, characterized by a specific grading curve, as illustrated in the previous Section, three irradiation tests are simulated. They differ for the radiation direction (along X, Y, and Z), and they are named Sample (1-3), respectively (Figure 3). On the irradiated surface the assumed fast and thermal neutron flux correspond to $3.2\times10^{10}\ \mathrm{n}/(\mathrm{cm}^2\cdot\mathrm{s})$ and $4.0\times10^{10}\ \mathrm{n}/(\mathrm{cm}^2\cdot\mathrm{s})$, respectively. Their kinetic energy is assumed to be 1 MeV, for fast neutrons, and 0.025 eV, for thermal neutrons. The temperature is set as $65^{\circ}\mathrm{C}$ on the same irradiated surface. The irradiation time is 24 hours. The average neutron fluxes and temperature on the analysed surfaces indicated

in Figure 3 are collected, together with the maximum tension and compression stress present on the mortar. These values are extracted for each studied sample to make a comparative analysis of the results in Figure 4.

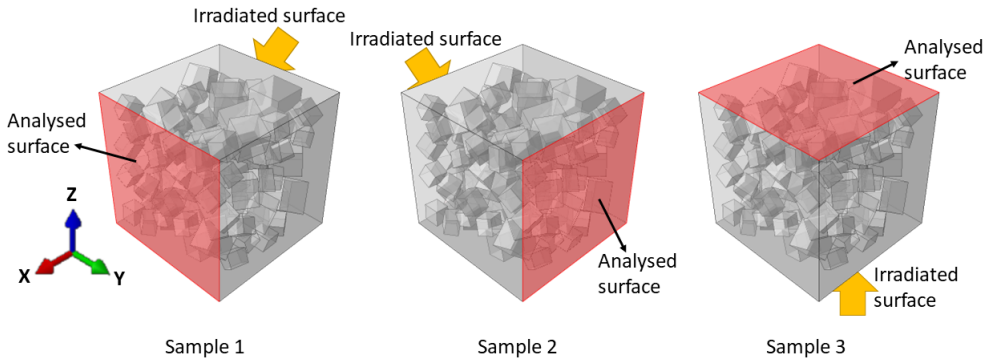

Figure 3: Simulated irradiation scenarios for each one of the three generated solid models.

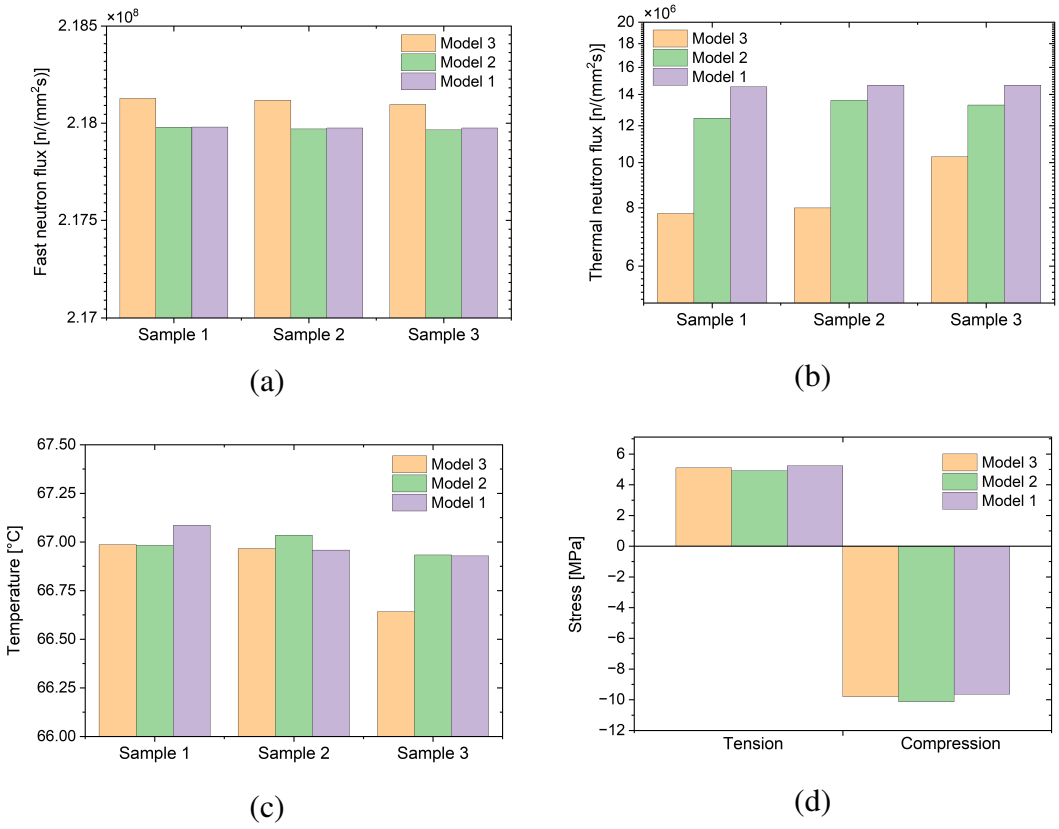

Figure 4: Results comparison: (a) fast neutron flux; (b) thermal neutron flux; (c) temperature; (d) stress.

Figure 4 (a-c) show, respectively, the results of the average fast and thermal neutron fluxes, and temperature on the analysed surfaces of the three samples indicated

in Figure 3, for each one of the models constructed as illustrated in Section 2.2. It is observed that the fast neutron flux is, practically, not influenced by the aggregate sieving (through the grading curve), nor by their distribution in space (through the different sample irradiation direction, along X, Y or Z). The fact that Model-3 in all the studied cases of irradiation direction exhibits slightly higher values, with respect to the other two models, can be attributed to the slightly lower aggregate volume fraction reached numerically for this realization, if compared to the other two solid models, that pertain to the other two different grading curves. In fact, from the aggregate phase concrete derives its shielding properties, therefore a higher improved (light) aggregate content must reflect into a higher shielding performance. From Figure 4 (b) it is clear that the thermal neutron flux is more affected by the aggregates sieving and distribution, than the fast group. The difference in the thermal neutron flux can reach nearly 50%, in reason of the aggregate grading curve (see variation of results among the three models, within a single sample). In the case of thermal neutrons, the realization characterized by a lower aggregate volume fraction (Model-3) is the one that indicates a lower absorption of this neutron group. Therefore, the associated flux is lower than for the other two models, as a result of a reduced transition of fast neutrons to thermal neutrons. This applies irrespective of the irradiation direction. This must be explained by the difference in the aggregate volume fraction between Model-1 and Model-2 (30.5%) with Model-3 (30%), more than by the difference in the sieving that distinguishes the models. This is supported, more clearly, by the results in terms of the fast flux. In fact, they are particularly in agreement to each other for the first two models, despite the difference in the sieving, than with Model-3. However, this aspect needs further investigation, and it will be object of future study.

The temperature difference among all samples is negligible, as shown in Figure 4 (c). This must be attributed to the limited dimension of the sample. It is significant, however, that the same representative elementary volume under study is, conversely, enough to detect some fluctuations in the neutron diffusive quantities. The total stress is also little affected by aggregate distribution and sieving (Figure 4 (d)), which is reassuring in relation to the fact that the composite can be considered macroscopically as isotropic. Due to the negligible amount of RIVE of the specific analysis, the detected total stress is expected to be due in large part to the thermal component. It partly depends on the thermal gradient between phases, and another part in the aggregate spatial distribution.

4 Concluding remarks

This work presents a comparative study on the effects of aggregate sieving and distribution on the shielding and thermo-mechanical performance of concrete employed in radiation shielding.

A coupled thermo-mechanical and neutron diffusion formulation, developed in the framework of the Finite Element Method, is proposed. The main governing equations of this procedure are introduced. They account for the estimate of the evolution in time

of the fast neutron and thermal neutron flux, temperature, and displacements/stress. The mathematical model takes into account the transition of fast neutrons to thermal neutrons; temperature rise caused by thermal neutron capture as a collateral effect; radiation induced volume expansion at the level of aggregates; and thermal expansion.

Mesoscale models in which the aggregates are represented as polyhedral inclusions, randomly distributed within mortar matrix are generated. Three different grading curves for the coarse aggregate fraction are simulated. For each one of these realizations, three radiation direction scenarios are considered, in order to analyze the influence of aggregate distribution in the diffusive processes taking place into concrete. The comparison between the simulated grading curves and the target Fuller curves shows good consistency with the input values represented by the aggregate volume fraction, and the nominal diameter distribution.

The numerical results show that the thermal neutron flux is influenced to some extent by the variation in grading curve, if compared to the fast neutron flux, and the other state variables. Specifically, it is proved that a slight variation in terms of the total reproduced volume fraction, with respect to the target one, contributes prominently on this discrepancy of results, and on the estimate of the overall shielding performance of concrete.

5 Acknowledgments

The financial support from the Ministry of Education of the People's Republic of China, China Scholarship Council (CSC) is gratefully acknowledged. The authors also acknowledge the support from the Italian Ministry of University and Research (MUR), in the framework of PRIN2017 Project 2017HFPKZY, and PRIN2020 Project 20209F3A37.

References

[1] Hilsdorf, H. K., J. Kropp, and H.J. Koch, "The effects of nuclear radiation on the mechanical properties of concrete." ACI Special Publication, 55, 223-254, 1978.

[2] T. Piotrowski, "Neutron shielding evaluation of concretes and mortars: A review", Construction and Building Materials, 277, 122238, 2021.

[3] B. Pomaro, F. Gramegna, R. Cherubini, V.D. Nadal, V. Salomoni, and F. Faleschini, "Gamma-ray shielding properties of heavyweight concrete with Electric Arc Furnace slag as aggregate: An experimental and numerical study", Construction and Building Materials, 200, 188-197, 2019.

[4] H.A. Baltas, M.U. Sirin, A. Celik, İ.L. Ustabas, and A. M. El-Khayatt, "Radiation shielding properties of mortars with minerals and ores additives", Cement and Concrete Composites, 97, 268-278, 2019.

[5] Y. Le Pape, “Structural effects of radiation-induced volumetric expansion on unreinforced concrete biological shields”, Nuclear Engineering and Design, 295, 534-548, 2015.
[6] Y. Jing, Y. Xi, “Modeling long-term distribution of fast and thermal neutron fluence in degraded concrete biological shielding walls”, Construction and Building Materials, 292, 123379, 2021.
[7] B. Pomaro, G. Xotta, V.A. Salomoni , C.E. Majorana, “A thermo-hydro-mechanical numerical model for plain irradiated concrete in nuclear shielding”, Materials and Structures, 55, 14, 2022.
[8] O. Gencel, W. Brostow, C. Ozel, M. Filiz, “An investigation on the concrete properties containing colemanite”, International Journal of Physical Sciences, 5, 216-225, 2010.
[9] M. Dabrowski, D. Jóźwiak-Niedźwiedzka, K. Bogusz, M.A. Glinicki, “Influence of serpentinite aggregate on the microstructure and durability of radiation shielding concrete”, Construction and Building Materials, 337, 127536, 2022.
[10] I. Maruyama, A. Sugie, “Numerical study on drying shrinkage of concrete affected by aggregate size”, Journal of Advanced Concrete Technology, 12, 279-288, 2014.
[11] H. Zhao, L. Zhang, Z. Wu, A. Liu, M. Imran, “Aggregate effect on the mechanical and fracture behaviours of concrete”, International Journal of Mechanical Sciences, 243, 108067, 2023.
[12] A.B.Azeez, K.S. Mohammed, A.V.Sandu, A.M.M. Al Bakri, H. Kamarudin, I. G. Sandu, “Evaluation of radiation shielding properties for concrete with different aggregate granule sizes”, Revista de Chimie, 64, 899-903, 2013.
[13] G. Mazzucco, B. Pomaro, G. Xotta, E. Garbin, V. Salomoni, and N. De Marchi, “Experimental and numerical characterization of normal-weight concrete at the mesoscale”, Journal of Materials in Civil Engineering, 34, 04022121, 2022.
[14] G. Mazzucco, B. Pomaro, G. Xotta, C.E. Maiorana, and V.A. Salomoni, “Tomography reconstruction of concrete materials for mesoscale modelling”, Engineering Computations, 37, 2275-2291, 2020.
[15] G. Mazzucco, B. Pomaro, V.A. Salomoni, C.E. Majorana, “Numerical modelling of ellipsoidal inclusions”, Construction and Building Materials, 167, 317-324, 2018.
[16] A. Un, Y. Sahin, “Determination of mass attenuation coefficients, effective atomic and electron numbers, mean free paths and kermas for PbO, barite and some boron ores”, Nuclear Instruments and Methods in Physics Research Section B: Beam Interactions with Materials and Atoms, 269, 1506-1511, 2011.
[17] E. Yılmaz, H. Baltas, E. Kırıs, İ.L. Ustabas, U.Ğ. Cevik, A.M. El-Khayatt, “Gamma ray and neutron shielding properties of some concrete materials”, Annals of Nuclear Energy”, 38, 2204-2212, 2011.
[18] L. Jin, X. Li, R. Zhang, X, Du, “Modelling of bond behavior of deformed bar embedded in concrete after heating to high temperatures: A mesoscale study”, Construction and Building Materials, 334, 127456, 2022.
[19] Z. Dong, Y. Chen, X. Wang, L. Kong, L. Wang, X. Li, F. Sun, “Evalua-

tion of thermophysical and mechanical properties of sandstone due to high-temperature", Materials, 15, 8692, 2022.